Second-order advantage with excitation-emission fluorescence spectroscopy and a flow-through optosensing device. Simultaneous determination of thiabendazole and fuberidazole in the presence of uncalibrated interferences

Gisela N. Piccirilli and Graciela M. Escandar*

Received 10th November 2009, Accepted 18th March 2010
First published as an Advance Article on the web 16th April 2010
DOI: 10.1039/b923565e

This paper presents a novel approach for the simultaneous determination of two widely used fungicides in a very interfering environment, combining the advantage of a spectrofluorimetric optosensor coupled to a flow-injection system and the selectivity of second-order chemometric algorithms. The sensor is based on the simultaneous retention of thiabendazole and fuberidazole on C18-bonded phase placed inside a flow-cell. After the arrival of the analytes to the sensing zone, the flow is stopped and the excitation-emission fluorescence matrix is read in a fast-scanning spectrofluorimeter. Parallel factor analysis (PARAFAC) and unfolded and multidimensional partial least-squares coupled to residual bilinearization (U- and N-PLS/RBL) were selected for data processing. These algorithms achieve the second-order advantage, and are in principle able to overcome the problem of the presence of unexpected interferences. The power of U-PLS/RBL to quantify both fungicides at parts-per-billion levels, even in the presence of high concentrations of spectral interferences such as carbaryl, carbendazim and 1-naphthylacetic acid, is demonstrated. Indeed, U-PLS/RBL allowed us to reach selectivity using a commercial but non-selective sensing support. To the best of our knowledge, this is the first time the potentiality of the 'second-order advantage' is evaluated on a flow-injection system, using an unspecific supporting material and in the presence of three real interferences. Using a sample volume of 2 mL, detection limits of 4 ng mL^{-1} and 0.3 ng mL^{-1} for thiabendazole and fuberidazol were respectively obtained in samples without interferences. In samples containing interferences, the limits of detection were 17 and 1 ng mL^{-1} for thiabendazole and fuberidazol, respectively. The sample frequency, including excitation/emission fluorescence matrix measurements, was 12 samples h^{-1}. The sensor was satisfactorily applied to the determination of both analytes in real water samples.

Introduction

Fungicides are a type of pesticides profusely used in agriculture with the purpose of controlling fungal diseases during the development of a crop, increasing its productivity, and improving the storage life and quality of harvested plants and crops.[1] Although fungicides are degraded through different pathways, they can accumulate in the environment if the rate of application exceeds the degradation rate. Thus, these residues can enter natural waters either directly or from drainage from agricultural lands, producing a detrimental effect over mammals and vegetables. Due to these facts, the control and quantification of compounds in environmental samples is of a great importance.[2,3]

Chromatographic methods are the most commonly employed for the quantification of fungicides and pesticides in general.[1,4–6] Spectroscopic methods have also been applied for this purpose, especially those based on luminescence signals.[7] In a previous paper, we carried out the determination of the fungicides carbendazim (MBC) and thiabendazole (TBZ) (Fig. 1) using fluorescence excitation-emission matrices obtained after the extraction of the analytes over a C18-membrane surface in a batch mode, and coupling these measurements with second-order algorithms.[8] In the latter work, two goals were achieved: 1) the power of the U-PLS/RBL algorithm to successfully predict the analyte concentrations in the presence of an inner-filter was demonstrated for the first time, and 2) the ability of this algorithm to overcome the interference produced by unsuspected species was established.

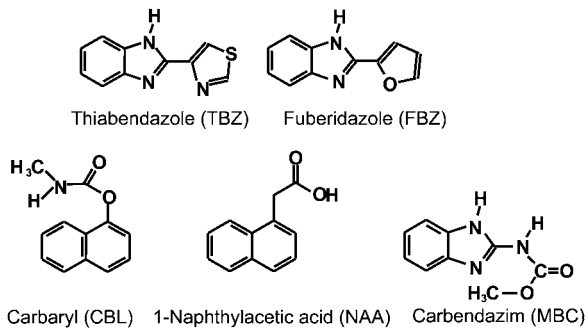

Fig. 1 Structures of thiabendazole, fuberidazole and potential interferences.

Instituto de Química Rosario (CONICET-UNR), Facultad de Ciencias Bioquímicas y Farmacéuticas, Universidad Nacional de Rosario, Suipacha 531, 2000 Rosario, Argentina. E-mail: escandar@iquir-conicet.gov.ar

On the basis of this previous experience, we decided to analyze the potentiality of second-order algorithms to process data obtained in a flow-through optosensing device, due to the well-known versatility and assembling easiness of flow injection systems, which are suitable for rapid and automatic analysis.[9] In the present work, TBZ and the widespread fungicide fuberidazole (FBZ, Fig. 1) are simultaneously retained in a commercially available packing material used as a flow-through sensing device, and then determined by EEFMs, directly recorded on the surface of the solid substrate. Flow-injection systems combined with solid-surface luminescence detection constitute a useful approach for the improvement of sensitivity and sampling frequency.[10–12] The group of Molina Díaz has developed different luminescence-based optosensors for the determination of both binary and ternary mixtures of different fungicides (benomyl, carbendazim, thiabendazole, o-phenylphenol, carbofuran, fuberidazole).[13–17] It is known that the spectral overlapping among the investigated analytes and/or foreign compounds, usually found in complex matrices, leads to decreased selectivity of the luminescence techniques. Resolution of overlapping luminescence profiles can be achieved, however, using multivariate calibration methods.

A flow-through optosensor spectrofluorimetric system combined with a first-order calibration approach (partial least-squares, PLS) was recently proposed for the resolution of mixtures of the pesticides 1-naphthol, o-phenylphenol and thiabendazole, using C18 silicagel as solid support.[18] However, the use of first-order data may not be the best way of resolving the problem of the presence of unexpected interferences in the samples. In these cases, some second-order multivariate calibration methods are, in principle, better suited for the successful resolution of these systems.[19,20] These latter methods achieve the so called "second-order advantage", which allows the quantitation of analytes even in the presence of unexpected sample constituents.[21,22] The first example of second-order advantage applied to a fluorescence optosensor was recently reported by Valero Navarro *et al.*, who determined 1- and 2-naphthylamines in the presence of 1-naphthalenemethylamine (interference) using a rather selective molecularly imprinted polymer (MIP)-fluorescence optosensing system.[23]

In the present paper, the determinations are carried out in solutions containing the analytes here studied and three agrochemicals selected as interferences (Fig. 1): carbaryl (CBL), 1-naphthylacetic acid (NAA) and MBC. Among the agrochemicals usually employed in our region, these latter compounds have solid-surface fluorescence spectra significantly overlapped with those of the studied analytes, and may be present in real water samples. In contrast to imprinted materials, such as MIPs or molecularly imprinted sol–gels, the commercial support selected in the present work is poorly selective. However, this problem is overcome when the method is assisted by second-order algorithms which achieve the second-order advantage. To the best of our knowledge, this is the first time that the potentiality of the 'second-order advantage' is evaluated on a flow-injection system with three real interferences. Three chemometric algorithms which achieve the second order advantage, namely, parallel factor analysis (PARAFAC),[24] unfolded partial least-squares coupled to residual bilinearization[25,26] (U-PLS/RBL), and multidimensional partial least-squares[27] coupled to residual bilinearization (N-PLS/RBL) are applied to process the solid-phase EEFMs.

Differences in the prediction capabilities of the employed algorithms are shown and discussed, and the advantages of working in a flow-through optosensor system are justified.

Finally, the feasibility of determining TBZ and FBZ in natural water samples is demonstrated.

Experimental

Reagents and solutions

All reagents were of high-purity grade and used as received. Thiabendazole and carbendazim were obtained from Riedel-de Haën. Fuberidazole, carbaryl and silica gel 100 C18-bonded phase (0.040–0.063 mm particle size) were purchased from Fluka. Methanol was obtained from Merck and 1-naphthylacetic acid was obtained from Sigma.

Stock solutions of thiabendazole (c.a. 300 μg mL^{-1}), fuberidazole (c.a. 300 μg mL^{-1}), carbaryl (c.a. 900 μg mL^{-1}) and carbendazim (c.a. 400 μg mL^{-1}) were prepared in methanol, and a stock solution of 1-naphthylacetic acid (c.a. 800 μg mL^{-1}) was prepared in acetone. These solutions are stable at 4 °C for at least four months. From these solutions, working aqueous solutions were prepared by taking appropriate aliquots, evaporating the organic solvent by use of dry nitrogen and diluting with water to the desired concentrations.

Apparatus

A Varian Cary-Eclipse luminescence spectrometer (Varian, Mulgrave, Australia) equipped with a xenon flash lamp was used to measure the optosensor response. A Gilson Minipuls-3 peristaltic pump (Villiers-Le-Ber, France), two six-port injection valves with exchangeable fixed volume loops, and a 25 μL inner volume quartz flow-through cell (Hellma 176.052-QS, Müllheim, Germany) packed with 25 mg of silica gel C18-bonded phase were employed to set-up the FIA manifold. PVC tubings of 0.76 mm i.d. were used for all connections. The cell was blocked at the outlet with some glass wool to prevent displacements of the silica gel C18 particles by the carrier, while the inlet of the flow-through cell was kept free.

Procedure

Two millilitres of sample solution containing the analytes, alone or in the presence of potential interferences, were inserted into the carrier stream (water) and pumped through the flow system at a flow rate of 2.0 mL min^{-1}. The spectrofluorimeter was set-up in its kinetic mode, using excitation and emission wavelengths of 300 and 350 nm, respectively, photomultiplier sensitivity of 600 V, and excitation and emission slit widths of 5 nm. When TBZ and FBZ arrived to the cell filled with the solid support, they were retained on it. When the maximum fluorescence signal was reached, the flow was stopped, the spectrofluorimeter was set-up in its scan 3D mode, and the corresponding EEFM was recorded using excitation and emission ranges of 250–316 nm (each 2 nm) and 325–400 nm (each 2 nm), respectively, and a scanning rate of 9600 nm min^{-1}. After these measurements, the kinetic mode was again selected, the flow was restored and both analytes were

desorbed from the flow-through cell with 500 μL of a 40% v/v methanol–water mixture which was injected in the FIA system by means of a second injection valve, and the signal returned to the baseline. The time elapsed between consecutive injections (including the fluorescence matrix measurement) was 5 min.

Chemometric analysis

Prior to the second-order calibration experiment, preliminary experiments indicated that, under the established working conditions (i. e., 2.0 mL of sample), linearity is held until 250 and 60 ng mL^{-1} for TBZ and FBZ, respectively, which were the limiting assayed concentrations in subsequent analyses.

A calibration set of 11 samples containing both analytes was prepared from the corresponding aqueous working solutions (Table 1). Nine samples of the set corresponded to the concentrations provided by a two-factor central composite design, and the remaining two samples contained only one of the studied analytes at an intermediate concentration (C_{TBZ} = 164 ng mL^{-1} and C_{FBZ} = 25.5 ng mL^{-1}). Each sample was subjected to the FIA procedure and the EEMF measurement described above.

A test set of 30 validation samples, different from the calibration ones, was prepared and processed in a similar way as the calibration solutions (Table 1). The obtained EEFMs were then analyzed with second-order multivariate calibration. The concentrations of both analytes were selected at random from the corresponding calibration ranges.

Table 1 Composition of the samples used in the calibration, validation and test sets

Calibration		Validation		Test	
TBZ/ ng mL^{-1}	FBZ/ ng mL^{-1}	TBZ/ ng mL^{-1}	FBZ/ ng mL^{-1}	TBZ/ ng mL^{-1}	FBZ/ ng mL^{-1}
51.3	25.5	97.5	36.0	128	22.5
277	25.5	103	45.0	72	30.0
164	1.2	170	12.5	140	30.0
164	49.5	10.0	10.5	200	15.0
83.1	8.4	97.5	10.5	155	4.0
246	8.4	36.0	36.0	51.5	3.8
83.1	43.5	154	0	128	21.5
246	43.5	97.5	36.0	72.0	22.0
164	25.5	97.5	60.0	150	24.0
164	0	0	10.5	155	3.0
0	25.5	36.0	60.0	90.0	24.0
		52.0	26.0	165	12.0
		83.5	1.4	231	12.0
		163	50.0	90.0	10.5
		154	1.1	210	2.7
		83.5	26.0	61.6	0
		246	43.0	10.0	14.0
		66.7	19.5	30.0	12.0
		83.5	50.0	20.0	0
		210	37.5	30.0	45.0
		149	30.0		
		0	19.5		
		82.0	30.0		
		36.0	10.0		
		80.0	6.0		
		50.0	37.5		
		123	48.0		
		62.0	1.5		
		100	33.5		
		245	44.0		

With the purpose of evaluating the method in the presence of three interfering agrochemicals, 20 samples containing random concentrations of the investigated analytes and high concentrations of CBL, NAA and MBC were evaluated. The levels of interferences (C_{CBL} = C_{NAA} = 6400 ng mL^{-1} and C_{MBC} = 2000 ng mL^{-1}) were within the range of the corresponding water solubilities. The fact that the highest concentrations for TBZ and FBZ were, respectively, 250 and 60 ng mL^{-1}, ensures that interferences were between 8 and 107 times more concentrated than these analytes.

Water sample procedure

The proposed methodology was applied for the quantification of both TBZ and FBZ in water samples in the presence of the interferences indicated above. Underground, tap, mineral and river water samples were prepared by spiking them with both analytes, obtaining concentration levels between 20 and 180 ng mL^{-1} for TBZ, and 3 and 40 ng mL^{-1} for FBZ. In addition, CBL, NAA and MBC were incorporated to these samples at the same concentrations used in the test samples. With the exception of river water samples, which were filtered through filter paper, the remaining water samples underwent no previous treatment.

Theoretical considerations

The selected algorithms (PARAFAC, U-PLS and N-PLS) are well known, and the coupling of U- and N-PLS with RBL has already been described in the literature.[25,26] Therefore, only a brief description is given.

It is first useful to consider the different manners in which these algorithms process three-way data arrays. For a given problem sample, PARAFAC builds a joint model, including the second-order signals for all the calibration samples and for the analyzed test sample data. This must be done for each of the test samples. In the first step of PARAFAC processing, the three-way array is decomposed, while in a second step the calibration concentrations are employed to estimate a given component concentration in the test sample. This means that a new PARAFAC model is calculated for each new problem sample to be predicted.

On the other hand, in the N-PLS/RBL and U-PLS/RBL methodologies, the first step consists of establishing a relationship between the measured calibration signals and the known calibration concentrations, without considering the test sample data. Once this is done, a postcalibration RBL procedure applied to the test sample signals is introduced, allowing one to model the presence of unexpected components and to accurately estimate the analyte concentration. In this way, PARAFAC resolves each component information separately, and this is the reason why second-order advantage is inherent to this model (the analyte signal is separated from that of the potential interferences). On the other hand, the remaining methods intend to find the relationship among the measured calibration responses and particular concentration information (used to build the model). This is why the potential interferences should be included in the calibration set of samples; otherwise a separate procedure, such as RBL, should be combined with the calibration model to obtain the second-order advantage.

The PARAFAC model

This algorithm often achieves the unique decomposition of three-dimensional data arrays, allowing concentrations and spectral profiles of sample components to be extracted. In fact, if EEFMs are arranged in a three-way array $\boldsymbol{F}$ of dimensions $I \times J \times K$, where I, J, and K are the number of samples, number of emission wavelengths, and number of excitation wavelengths, respectively, PARAFAC attempts to decompose it into three matrices $\mathbf{A}$ (scores), $\mathbf{B}$, and $\mathbf{C}$ (loadings) with elements a_{in}, b_{jn}, c_{kn}, respectively, where n indicates the number of component. An element of $\boldsymbol{F}$ is given by:

$$F_{ijk} = \sum_{n=1}^{N} a_{in} b_{jn} c_{kn} + e_{ijk} \quad (1)$$

where F_{ijk} is the fluorescence intensity for sample i at the emission wavelength j and excitation wavelength k and e_{ijk} indicates an element of the array $\boldsymbol{E}$, which collects the variability not accounted by the model. For a given component n, the elements a_{in}, b_{jn}, and c_{kn} are arranged in the score vector $\mathbf{a}_n$ (whose elements are directly proportional to the component concentrations in each sample) and the loading vectors $\mathbf{b}_n$ and $\mathbf{c}_n$, which estimate its emission and excitation profiles, respectively. The array of EEFM data is fitted to eqn (1) by least-squares. Although ambiguities remain in the absolute component concentrations and chemical identities of the components, they can be solved by using training samples of known concentration and comparing the individual excitation and emission profiles with those of standards. As was indicated above, PARAFAC achieves the second-order advantage combining data from calibration and test samples before computing the regression coefficients.

The U-PLS/RBL model

In the U-PLS method, second-order data are unfolded into vectors before PLS is applied. The I_{cal} calibration data matrices are first vectorized into $JK \times 1$ vectors, and then a usual PLS model is built using these data together with the vector of calibration concentrations $\mathbf{y}$ (size $I_{\mathrm{cal}} \times 1$). This provides a set of loadings $\mathbf{P}$ and weight loadings $\mathbf{W}$ (both of size $JK \times A$, where A is the number of latent factors), as well as regression coefficients $\mathbf{v}$ (size $A \times 1$). If no unexpected components occurred in the unknown sample, $\mathbf{v}$ could be employed to estimate the analyte concentration according to:

$$y_{\mathrm{u}} = \mathbf{t}_{\mathrm{u}}{}^{\mathrm{T}}\mathbf{v} \quad (2)$$

where $\mathbf{t}_{\mathrm{u}}$ is the unknown sample score, obtained by projecting the vectorized data for the unknown sample $\mathrm{vec}(\mathbf{X}_{\mathrm{u}})$ onto the space of the A latent factors:

$$\mathbf{t}_{\mathrm{u}} = (\mathbf{W}^{\mathrm{T}}\mathbf{P})^{-1}\mathbf{W}^{\mathrm{T}}\mathrm{vec}(\mathbf{X}_{\mathrm{u}}) \quad (3)$$

where $\mathrm{vec}(\cdot)$ implies the vectorization operator and $\mathbf{X}_{\mathrm{u}}$ is the unknown sample matrix. When unexpected constituents occur in $\mathbf{X}_{\mathrm{u}}$, then the sample scores given by eqn (3) are unsuitable for analyte prediction through eqn (2). In this case, the residuals of the U-PLS prediction step [s_{p}, see eqn (4) below] will be abnormally large in comparison with the typical instrumental noise level:

$$s_{\mathrm{p}} = \|\mathbf{e}_{\mathrm{p}}\|/(JK - A)^{1/2} = \|\mathrm{vec}(\mathbf{X}_{\mathrm{u}}) - \mathbf{P}(\mathbf{W}^{\mathrm{T}}\mathbf{P})^{-1}\mathbf{W}^{\mathrm{T}}\mathrm{vec}(\mathbf{X}_{\mathrm{u}})\|/(JK - A)^{1/2} = \|\mathrm{vec}(\mathbf{X}_{\mathrm{u}}) - \mathbf{P}\mathbf{t}_{\mathrm{u}}\|/(JK - A)^{1/2} \quad (4)$$

where $\|\cdot\|$ indicates the Euclidean norm.

This situation can be handled by RBL, which aims at minimizing the norm of the residual vector $\mathbf{e}_{\mathrm{u}}$, computed while fitting the sample data to the sum of the relevant contributions:

$$\mathrm{vec}(\mathbf{X}_{\mathrm{u}}) = \mathbf{P}\,\mathbf{t}_{\mathrm{u}} + \mathrm{vec}[\mathbf{B}_{\mathrm{unx}}\,\mathbf{G}_{\mathrm{unx}}\,(\mathbf{C}_{\mathrm{unx}})^{\mathrm{T}}] + \mathbf{e}_{\mathrm{u}} \quad (5)$$

where $\mathbf{B}_{\mathrm{unx}}$ and $\mathbf{C}_{\mathrm{unx}}$ are matrices containing the first left and right eigenvectors of $\mathbf{E}_{\mathrm{p}}$, and $\mathbf{G}_{\mathrm{unx}}$ is a diagonal matrix containing its singular values, as obtained from singular value decomposition (SVD) analysis:

$$\mathbf{B}_{\mathrm{unx}}\,\mathbf{G}_{\mathrm{unx}}\,(\mathbf{C}_{\mathrm{unx}})^{\mathrm{T}} = \mathrm{SVD}(\mathbf{E}_{\mathrm{p}}) \quad (6)$$

where $\mathbf{E}_{\mathrm{p}}$ is the $J \times K$ matrix obtained after reshaping the $JK \times 1$ $\mathbf{e}_{\mathrm{p}}$ vector of eqn (4) and SVD indicates taking the first principal components.

During this RBL procedure, $\mathbf{P}$ is kept constant at the calibration values, and $\mathbf{t}_{\mathrm{u}}$ is varied until $\|\mathbf{e}_{\mathrm{u}}\|$ is minimized in eqn (5) using a Gauss-Newton procedure. Once $\|\mathbf{e}_{\mathrm{u}}\|$ is minimized, the analyte concentrations are provided by eqn (2), by introducing the final $\mathbf{t}_{\mathrm{u}}$ vector found by the RBL procedure.

We notice that the aim which guides the RBL procedure is the minimization of the residual error s_{u} to a level compatible with the degree of noise present in the measured signals, with s_{u} given by:

$$s_{\mathrm{u}} = \|\mathbf{E}_{\mathrm{u}}\|/[(J - N_{\mathrm{RBL}})(K - N_{\mathrm{RBL}}) - A]^{1/2} \quad (7)$$

where N_{RBL} is the number of RBL components and A the number of calibration PLS factors. Therefore, if more than one unexpected component is considered, RBL should select the simplest model giving a residual value which is not statistically different than the minimum one.

We note that two different residual parameters appear in the above discussion, which should not be confused: s_{p} [eqn (4)] corresponds to the difference between the unknown sample signal and that model by U-PLS *before* the RBL procedure, while s_{u} [eqn (7)] arises from the difference *after* the RBL modeling of the interferent effects. Hence it is the latter one which should be comparable to the instrumental noise level if RBL is successful.

The N-PLS/RBL model

The N-PLS method applied to second-order data is similar to the unfolded U-PLS method, but original data matrices are not unfolded. During the calibration phase, two sets of loadings $\mathbf{W}^{\mathrm{j}}$ and $\mathbf{W}^{\mathrm{k}}$ are obtained (of sizes $J \times A$ and $K \times A$, where A is the number of latent factors), as well as a vector of regression coefficients $\mathbf{v}$ (size $A \times 1$). The prediction expression is analogous to eqn (2) when no unexpected components occur in the unknown sample. In the presence of unexpected constituents, the sample scores are unsuitable for analyte prediction. The residuals of the N-PLS modeling of the unknown sample signal [s_{p}, see eqn (8)

below] will be abnormally large in comparison with the typical instrumental noise level:

$$s_p = \|\mathbf{e}_p\|/(JK - A)^{1/2} = \|\mathrm{vec}(\mathbf{X}_u) - \mathrm{vec}(\hat{\mathbf{X}}_u)\|/(JK - A)^{1/2} \quad (8)$$

where $\hat{\mathbf{X}}_u$ is the sample data matrix ($\mathbf{X}_u$) reconstructed by the N-PLS model.

The situation is handled in a manner similar to that discussed for U-PLS/RBL, minimizing the residuals computed while fitting the sample data to the sum of the relevant contributions:

$$\mathbf{X}_u = \mathrm{reshape}\{\mathbf{t}_u[(\mathbf{W}^j|\otimes|\mathbf{W}^k)]\} + \mathrm{SVD}(\hat{\mathbf{X}}_u - \mathbf{X}_u) + \mathbf{E}_u \quad (9)$$

where 'reshape' indicates transforming a $JK \times 1$ vector into a $J \times K$ matrix, and $|\otimes|$ is the Kathri-Rao operator. During this RBL procedure, the weight loadings $\mathbf{W}^j$ and $\mathbf{W}^k$ are kept constant at the calibration values, and $\mathbf{t}_u$ is varied until the final RBL residual error s_u is minimized using a Gauss-Newton procedure, with s_u given by an equation analogous to (7). Once this is done, the analyte concentrations are provided by an equation analogous to (2), by introducing the final $\mathbf{t}_u$ vector found by the RBL procedure.

Software

The routines employed for PARAFAC, U-PLS, and N-PLS are written in MATLAB 7.0[28] and are available on the Internet.[29] These algorithms were implemented using the graphical interface of the MVC2 toolbox,[30] which is also available on the Internet.[31] This latter toolbox implements the N-PLS/RBL and U-PLS/RBL methods for studying the effect produced by interferences.

Results and discussion

The use of silica gel C18 as a fluorescence optosensor for both TBZ and FBZ combined with zero-order calibration methods has already been described.[14,16,32] Owing to the non-polar nature of the support, complete retention occurs when the analytes are in their neutral forms. The deprotonation constant values reported for TBZ ($pK_a1 \approx 0.5$, $pK_a2 = 4.8$, $pK_a3 = 11.3$)[33] and FBZ ($pK_a1 = 5.0$ and $pK_a2 = 11.7$)[34] indicate that at a neutral pH both molecules remain in their uncharged structures. Therefore, pure water was selected both as carrier and for the working solutions. Although TBZ shows higher fluorescence signals near pH 2,[35] the emission at neutral pH is high enough to be easily measured from the studied solid support. On the other hand, the optimum pH value for the fluorescence of FBZ is in the range 6–10.[35]

Fig. 2 shows the fluorescence excitation and emission spectra for TBZ and FBZ, adsorbed on the C18 solid surface. It is clear in this figure that overlapping occurs among the excitation and the emission spectra and the background signal, which hinders the direct spectrofluorimetric determination of both analytes. As will be discussed below, the situation becomes more serious if other agrochemicals are concomitantly retained in the support and fluoresce in the same spectral region of the investigated analytes (Fig. 2). Hence, with the purpose of overcoming the problem of the spectral overlapping between the analytes and also among the analytes and interferences, chemometric analysis with algorithms which achieve the second-order advantage was applied. The selection of the second-order algorithms was made with the objective of testing the very popular PARAFAC model, which was already applied for the determination of TBZ, FBZ and MBC in methanolic synthetic samples in the absence of interferences,[36] and two latent structured algorithms which are being increasingly applied such as U-PLS/RBL and multidimensional N-PLS/RBL.[22] According to our experience, these latter models provided very satisfactory results in the resolution of complex systems.[8,37–39] The results are discussed in the following sections.

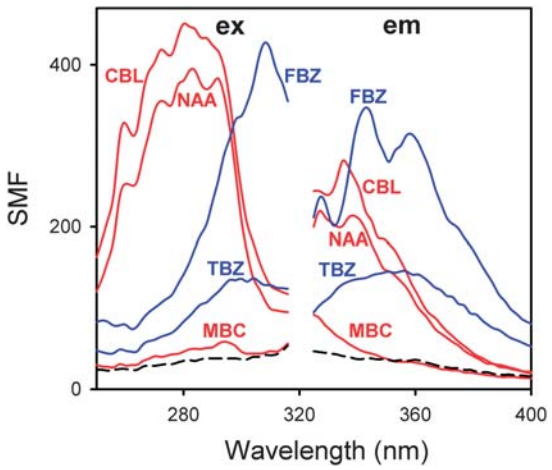

Fig. 2 Solid matrix fluorescence (SMF) excitation (ex) and emission (em) spectra for TBZ and FBZ (blue solid lines), and for CBL, NAA and MBC (red solid lines) immobilized onto silica gel C18. The dashed black lines correspond to the background signals. $C_{TBZ} = 100$ ng mL^{-1}; $C_{FBZ} = 19.5$ ng mL^{-1}; $C_{CBL} = C_{NAA} = 6400$ ng mL^{-1}; $C_{MBC} = 2000$ ng mL^{-1}. In all cases, λex = 300 nm and λem = 340 nm.

Validation samples

In order to build a second-order calibration model, EEFMs were recorded for the calibration samples. The employed spectral ranges, 325–358 nm (emission) and 270–312 (excitation) for both TBZ and FBZ, were selected after a suitable consideration of the spectral regions corresponding to their maximum signals, and avoiding potentially problematic regions where the analytes showed similar spectral profiles. Fig. 3A shows the contour plots of the EEFMs for TBZ, FBZ and the silica gel C18 background, in the final selected wavelength ranges. For clarity these plots are shown separately.

PARAFAC was applied to three-way data arrays built by joining the data matrices for each of the validation samples in turn, with those for the set of calibration samples. PARAFAC was initialized with the loadings giving the best fit after a small number of trial runs, selected from the comparison of the results provided by generalized rank annihilation and several orthogonal random loadings.[40] The number of responsive components to be included in the model was selected by the so-called core consistency analysis.[41] The estimated number of components using the above technique was two, which is justified taking into account the presence of both investigated compounds and the application of a mean centering procedure which avoids the background contribution to the signals.

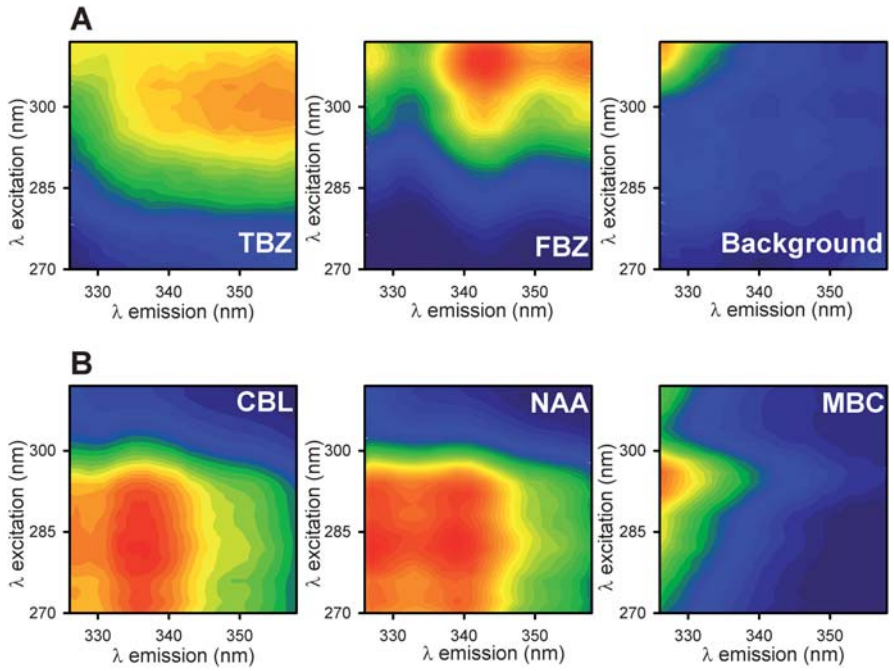

Fig. 3 Two-dimensional contour plots of the excitation-emission fluorescence matrices for typical samples containing the studied analytes (A), and the interferences (CBL, NAA and MBC) as indicated (B). $C_{TBZ} = 100$ ng mL^{-1}; $C_{FBZ} = 19.5$ ng mL^{-1}; $C_{CBL} = C_{NAA} = 6400$ ng mL^{-1}; $C_{MBC} = 2000$ ng mL^{-1}.

Fig. 4A and B show the prediction results for TBZ and FBZ, respectively, corresponding to the application of PARAFAC to a set of 30 validation samples. Although some prediction values for TBZ are rather disperse (Fig. 4A), the strong spectral overlapping between both analytes and the notable difference of their quantum efficiencies (see Fig. 2) led us to conclude that the results are acceptable. This conclusion is reflected in both the corresponding RMSEP (root-mean-square error of prediction) and REP (relative error of prediction) values (Table 2), and also in Fig. 4C, where the elliptical joint confidence region (EJCR)[42] for the slope and intercept of the found *vs.* nominal value plot for TBZ is shown. It is notable that while the ellipse for FBZ (red solid line in Fig. 4D) includes the theoretically expected values of (1,0), indicating accuracy of the developed methodology for this analyte, the ideal (1,0) point remains close but outside the TBZ ellipse (Fig. 4C), denoting poorer prediction accuracy for TBZ.

With the purpose of estimating the number of optimum latent variables for both U- and N-PLS, leave-one-sample-out cross-validation was performed.[43] The optimum number of factors is estimated by calculating the ratios $F(A) = \text{PRESS}(A < A^*)/\text{PRESS}(A)$, where $\text{PRESS} = \Sigma(c_{i,\text{act}} - c_{i,\text{pred}})^2$, A is a trial number of factors, A^* corresponds to the minimum PRESS, and $c_{i,\text{act}}$ and $c_{i,\text{pred}}$ are the actual and predicted concentrations for the ith sample left out of the calibration during cross validation, respectively. Then, the number of factors leading to a probability of less than 75% that $F > 1$ is selected. This analysis led to the conclusion that the latter number is 2 for the most cases, as expected for this system using a mean centering procedure, with the exception of the A value for TBZ processed with U-PLS ($A = 3$, see Table 3). Apparently, U-PLS needs an additional component to correctly model the TBZ profile.

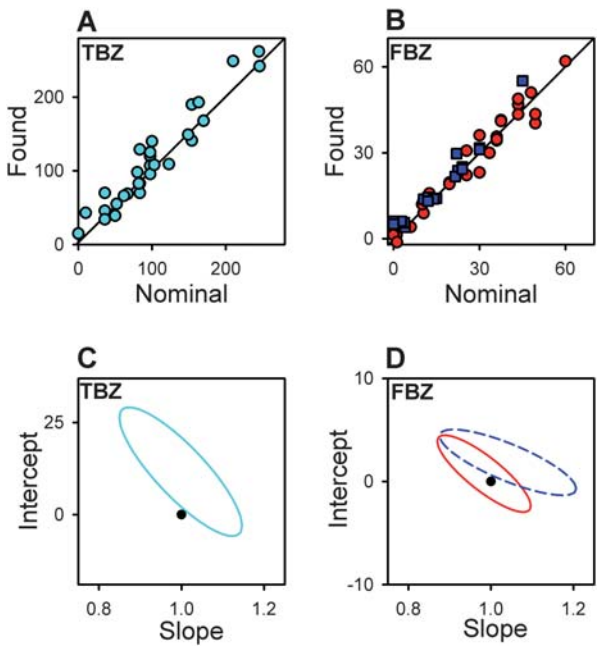

Fig. 4 Plots for PARAFAC predicted concentrations as a function of the nominal values for (A) TBZ in validation samples (cyan circles), and for (B) FBZ in validation samples (red circles) and in samples with interferences (blue squares). In (A) and (B) the solid lines are the perfect fits. Elliptical joint regions (at 95% confidence level) for the slopes and intercepts of the regressions of (C) TBZ validation data (cyan solid line), and of (D) FBZ validation data (red solid line) and the test data (blue dashed line). Black points in (C) and (D) mark the theoretical (intercept = 0, slope = 1) points. $C_{CBL} = C_{NAA} = 6400$ ng mL^{-1}; $C_{MBC} = 2000$ ng mL^{-1}.

Table 2 Statistical results for TBZ and FBZ in validation samples and in samples with CBL, NAA and MBC as interferences

	PARAFAC		U-PLS		N-PLS	
	TBZ	FBZ	TBZ	FBZ	TBZ	FBZ
Validation samples[a]						
RMSEP/ng mL^{-1}[b]	21	4	16	3	22	3
REP (%)[c]	14	20	10	15	15	17
LOD/ng mL^{-1}[d]	4	0.3	4	0.3	4	0.3
			U-PLS/RBL		**N-PLS/RBL**	
Samples with interferences[e]						
RMSEP/ng mL^{-1}[b]	[f]	4	14	3	[f]	3
REP (%)[c]	[f]	20	9	15	[f]	15
LOD/ng mL^{-1}[d]	[f]	0.6	17	1	[f]	1

[a] Number of samples = 30. [b] RMSEP, root-mean-square error of prediction. [c] REP, relative error of prediction. [d] LOD, limit of detection and calculated according to ref. 37. [e] Number of samples = 20. [f] See text.

Fig. 5 (A and B) and 6 (A and B) show the prediction results corresponding to the application of U-PLS and N-PLS, respectively, to the same set of 30 validation samples analysed above, and Fig. 5 (C and D) and 6 (C and D) show the corresponding ellipses of the EJCR analyses. In Table 2 the obtained statistical results are collected. Comparison of the results obtained from U-PLS with those obtained by applying both N-PLS and PARAFAC to the validation samples shows that the former renders results slightly better for both analytes. Limits of detection are also slightly better using U-PLS.

Samples containing unexpected agrochemicals

The usefulness of the proposed method will be more appreciated when its capacity to overcome the ubiquitous problem of the potential presence of interfering species in the analyzed matrices is demonstrated. Consequently, the determination of the fungicides under study was carried out in the presence of other agrochemicals, which could be concomitantly present in new samples but not in the calibration ones. In a previous work,[8] it was reported that TBZ, FBZ, CBL, NAA and MBC show fluorescence signals in a C18 support, and a significant overlapping among them is verified (Fig. 2 and 3B). In fact, if the structures of the foreign compounds are analyzed at the neutral working pH, it can be concluded that CBL (which loses the proton of the secondary amine at acid pH)[44] and MBC ($pK_a1 = 4.3$ and $pK_a2 = 10.8$)[45] remain in their neutral configurations. On the other hand, although NAA, with a pK_a value of 4.26,[46] is mainly present in its dissociated form at the neutral working pH, it is partially retained in the support, leading to a fluorescence signal overlapped with those of the studied compounds. Fig. 3B shows the individual contour plots of the EEFMs for the three interferences in the selected wavelength ranges.

Twenty test samples containing the studied analytes and CBL, NAA and MBC were prepared according to the discussion presented in the experimental section and were evaluated with PARAFAC, U-PLS/RBL and N-PLS/RBL algorithms.

The selection of PARAFAC factors for these samples was carried out through the analysis of PARAFAC residuals,[24] and the spectral profiles produced by the addition of subsequent components. In the latter test, if the addition of a new component

Table 3 Cross-validation results for calibration samples using U-PLS and N-PLS[a]

TBZ					FBZ				
U-PLS									
A	PRESS/(ng mL^{-1})^2	RMSECV/ng mL^{-1}	*F*	*p*	*A*	PRESS/(ng mL^{-1})^2	RMSECV/ng mL^{-1}	*F*	*p*
1	7.7×10^4	83.8	95.9	0.999	1	1.6×10^2	3.8	9.9	0.999
2	4.8×10^3	20.9	5.9	0.996	**2**	**15.7**	**1.2**	**1.0**	**0.499**
3	$\mathbf{9.4 \times 10^2}$	**9.2**	**1.2**	**0.599**	3	28.6	1.6	—	—
4	8.1×10^2	8.5	1.0	0.499	4	18.0	1.3	—	—
5	8.5×10^2	8.8	—	—	5	16.9	1.2	—	—
6	8.8×10^2	8.9	—	—	6	17.0	1.2	—	—
7	8.7×10^2	8.9	—	—	7	17.2	1.2	—	—
8	8.7×10^2	8.9	—	—	8	17.2	1.2	—	—
N-PLS									
1	8.0×10^4	85.2	75.1	0.999	1	1.9×10^2	4.1	9.2	0.999
2	$\mathbf{1.4 \times 10^3}$	**11.4**	**1.3**	**0.681**	**2**	3.1×10^1	**1.6**	**1.5**	**0.750**
3	1.1×10^3	9.8	1.0	0.499	3	2.3×10^1	1.4	1.1	0.578
4	1.3×10^3	10.8	—	—	4	2.4×10^1	1.5	1.2	0.617
5	1.8×10^3	12.6	—	—	5	2.0×10^1	1.4	1.0	0.499
6	1.9×10^3	13.0	—	—	6	2.3×10^1	1.4	—	—
7	1.9×10^3	13.3	—	—	7	2.6×10^1	1.5	—	—
8	2.0×10^3	13.6	—	—	8	2.6×10^1	1.5	—	—

[a] All symbols have been defined in the text, except *p* (probability) and RMSECV (root-mean-square error of cross-validation). Optimum values are shown in boldface.

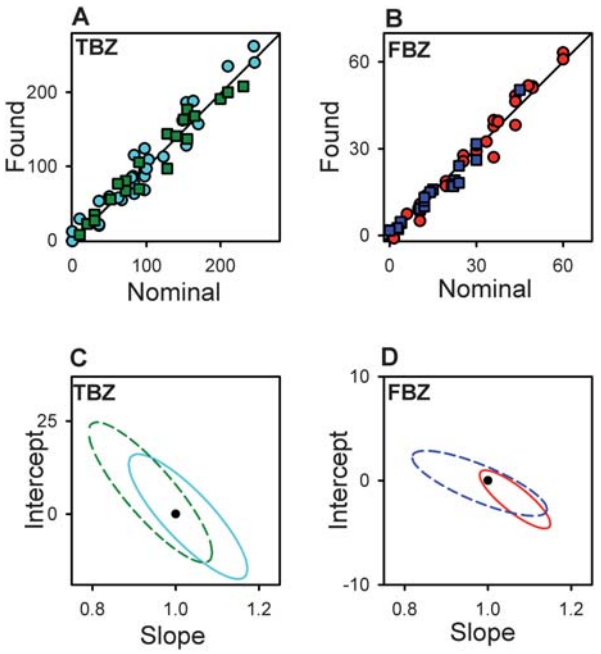

Fig. 5 Plots for U-PLS or U-PLS/RBL predicted concentrations as a function of the nominal values for (A) TBZ in validation samples (cyan circles) and in samples with interferences (green squares), and for (B) FBZ in validation samples (red circles) and in samples with interferences (blue squares). In (A) and (B) the solid lines are the perfect fits. Elliptical joint regions (at 95% confidence level) for the slopes and intercepts of the regressions for (C) TBZ validation (cyan solid line) and test (green dashed line) data, and for (D) FBZ validation (red solid line) and test (blue dashed line) data. Black points in (C) and (D) mark the theoretical (intercept = 0, slope = 1) points. $C_{CBL} = C_{NAA} = 6400$ ng mL^{-1}; $C_{MBC} = 2000$ ng mL^{-1}.

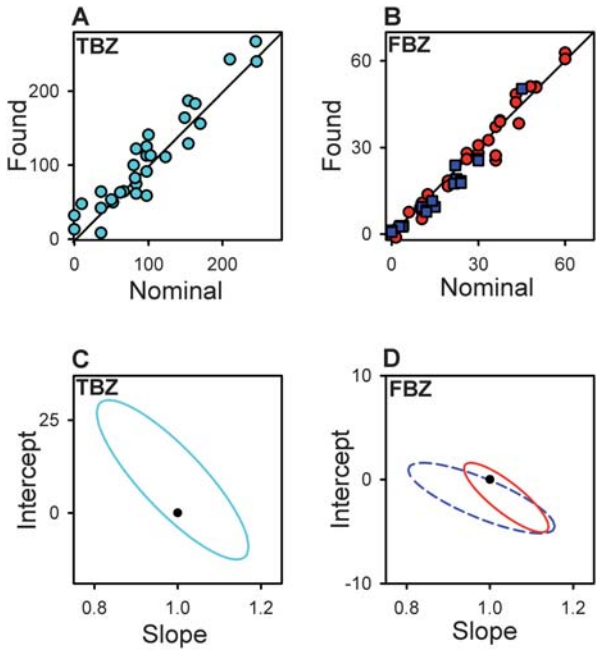

Fig. 6 Plots for N-PLS or N-PLS/RBL predicted concentrations as a function of the nominal values for (A) TBZ in validation samples (cyan circles), and for (B) FBZ in validation samples (red circles) and in samples with interferences (blue squares). In (A) and (B) the solid lines are the perfect fits. Elliptical joint regions (at 95% confidence level) for the slopes and intercepts of the regressions for (C) TBZ validation data (cyan solid line), and for (D) FBZ validation data (red solid line) and the test data (blue dashed line). Black points in (C) and (D) mark the theoretical (intercept = 0, slope = 1) points. $C_{CBL} = C_{NAA} = 6400$ ng mL^{-1}; $C_{MBC} = 2000$ ng mL^{-1}.

generated repeated profiles, suggesting overfitting, the new component was discarded and the previous number of components (*i.e.*, the last one which did not produce overfitting) was selected. The results obtained established that the number of total components required by PARAFAC in samples with the studied interferences was three. This fact suggests that the algorithm considers the three new compounds as a single mathematical component, which could be justified on the basis of the similar spectral profiles for NAA and CBL and the low intensity of the completely overlapped signal of MBC (see Fig. 2).

The TBZ prediction ability of PARAFAC in samples with interferences was worse than that obtained in the validation samples, and these results were therefore not considered. However, the predictions for FBZ were in good agreement with the nominal values (blue squares in Fig. 4C). The bad TBZ recoveries obtained with PARAFAC, especially in samples with low TBZ concentration, may be ascribed to a lack of selectivity for this constituent in these latter complex samples.

When U- and N-PLS/RBL algorithms were applied to the test samples, in addition to the number of latent variables estimated for the calibration set for TBZ and FBZ, these samples required the introduction of the RBL procedure with two unexpected components in most cases. Adding more unexpected components did not improve the fit, indicating that U- and N-PLS/RBL algorithms model the profiles of the three interferences using two principal components.

N-PLS/RBL allows for a good prediction of FBZ concentrations in samples with a high level of interferences (blue squares in Fig. 6B and blue dashed line in Fig. 6D), but it is unable to correctly determine TBZ in these samples.

On the other hand, Fig. 5A (green squares) and 5B (blue squares) illustrate the prediction values corresponding to the application of U-PLS/RBL to the test samples. As can be concluded, in this case the predictions for both TBZ and FBZ are in good agreement with the nominal values. If the EJCRs for the slope and intercept of the above plots are analyzed (Fig. 5C and 5D, green and blue dotted lines respectively), we conclude that the ellipses include the theoretically expected point (1,0) suggesting a high-quality prediction. The statistical results shown in Table 2, with adequate values for RMSEP and REP values for both analytes, do also support this conclusion. As regards the corresponding LODs (17 and 1 ng mL^{-1} for TBZ and FBZ, respectively), although these values are larger than those obtained in the absence of interferences (4 and 0.3 ng mL^{-1}), they are acceptable taking into account that a simple methodology is applied to a complex sample.

In comparing the LOD for TBZ using the flow-through optosensor methodology ($LOD_{TBZ} = 4$ ng mL^{-1}) with that previously obtained by our group in a batch system ($LOD_{TBZ} = 0.2$ ng mL^{-1}),[8] one may state that although the methodology now proposed achieves a lower detection capability, working in a batch mode involves a significant larger sample volume (25000 μL *vs.* 2000 μL) and restricted automation possibilities.

Table 4 Recovery study of mixtures of TBZ and FBZ in spiked water samples in the presence of CBL, NAA and MBC, using solid-phase EEFMs and U-PLS/RBL[a]

	TBZ				FBZ			
	Taken/ng L^{-1}	Found[b]/ng L^{-1}	Recovery/%	t^c	Taken/ng L^{-1}	Found[b]/ng L^{-1}	Recovery/%	t^c
Mineral water[d]	35.9	39 (5)	109		28.5	30.7 (0.3)	108	
	120	125 (1)	104		10.2	10.1 (0.5)	99	
	154	158 (9)	103	1.66	6.0	4.2 (0.3)	70	0.69
Tap water[e]	56.0	59 (6)	105		22.5	23.3 (0.5)	104	
	75.0	96 (4)	128		21.0	23.9 (0.8)	114	
	150	151 (1)	101	1.27	10.5	10.9 (0.7)	104	2.02
Underground water[f]	56.5	53 (1)	95		6.0	8.6(0.1)	143	
	100	79 (2)	79		3.0	4.7 (0.1)	156	
	180	168 (9)	93	2.11	18.0	17.7 (0.2)	98	1.85
River water[g]	25.6	15 (5)	59		14.0	16.2 (0.5)	116	
	56.5	54 (5)	96		6.0	4.4 (0.4)	73	
	180	163 (9)	91	1.56	18.0	19.7 (0.2)	109	0.08
River water[h]	20.0	22 (5)	110		40.0	39 (1)	98	
	56.5	52 (7)	92		34.5	34.0 (0.6)	99	
	180	162(4)	90	0.47	6.0	6.1 (0.3)	102	0.87

[a] $C_{CBL} = 2000$ ng mL^{-1} and $C_{NAA} = C_{MBC} = 6400$ ng mL^{-1}. [b] Mean of duplicates. Standard deviation between parentheses. [c] Calculated student t for the average recovery. The critical t value for $n - 1$ degrees of freedom and at a 95% significance level is $t_{crit(0.05,2)} = 4.30$ (see text). [d] From Villavicencio hills (Mendoza, Argentina). This water contains $NaHCO_3$ (350 μg mL^{-1}), $Ca(HCO_3)_2$ and $Mg(HCO_3)_2$ (259 μg mL^{-1}), Na_2SO_4, $CaSO_4$ and $MgSO_4$ (234 μg mL^{-1}), NaCl, $CaCl_2$ and $MgCl_2$ (47 μg mL^{-1}), CaF_2 (1.4 μg mL^{-1}) and oligoelements (1.5 μg mL^{-1}). [e] From Rosario City (Santa Fe, Argentina). [f] From the surroundings of Funes City (Santa Fe, Argentina). [g] Paraná river (Argentina). [h] Carcarañá river (Argentina).

Because previously reported systems based on flow-through optosensors with C18 silica gel as solid support involve other agrochemical mixtures and were developed in different working conditions, it is difficult to make an objective comparison with the presently proposed optosensor. However, some literature values of LOD for TBZ or FBZ are worth mentioning. Using 40 μL of a binary sample of TBZ and warfarin, an LOD of 2.35 ng mL^{-1} for TBZ was obtained.[47] Injecting a sample volume of 2,100 μL of a ternary mixture, an LOD of 0.09 ng mL^{-1} for FBZ was reported.[16] Following a similar procedure, LODs of 0.31 and 0.08 ng mL^{-1} were obtained for TBZ, using 600 and 3200 μL, respectively, of binary samples.[14] By using a sample volume of 2600 μL, a system formed by TBZ and *o*-phenylphenol rendered an LOD of 0.09 ng mL^{-1} for TBZ. Very recently, TBZ was determined in mixtures of this analyte and the herbicide metsulfuron methyl, and LODs of 2.5 and 6.0 ng mL^{-1} were estimated respectively, using volumes of 2060 and 300 μL.[32] As a conclusion, the presently obtained LOD is within the range of those reported by other authors. However, the main advantage of our proposal is its high selectivity, due to the valuable coupling of the instrumental measurements with an appropriate second-order algorithm.

Real water samples

In view of the above results, U-PLS/RBL was selected as the algorithm to be applied to real samples. The estimated concentrations of the studied fungicides in natural waters are at parts-per-billion levels, and higher concentrations could be found in farming areas.[48,49] Therefore, in principle, the proposed method could be used to determine the fungicides without the necessity of applying a pre-concentration step. A recovery study by spiking waters of different origins with TBZ, FBZ and the three interferent agrochemicals was carried out (Table 4). The average recovery of both TBZ and FBZ in each type of water at the three different fortification levels was tested for significance by using the Student *t*-test: the null hypothesis corresponds to the recovery of 100%.[42] The t values obtained for $n - 1$ degrees of freedom (where n is the number of evaluated levels) at a 95% of significance compare favourably with the corresponding tabulated value [$t_{crit(0.05,2)} = 4.30$], suggesting that the proposed method is appropriate for the simultaneous determination of TBZ and FBZ. The obtained results suggest that neither the investigated foreign agrochemicals nor other inorganic and organic compounds which may be possibly present in the studied samples produce a significant interference in our analysis.

Conclusions

In the present article, a flow-through optosensor is developed, suitable for the simultaneous quantification of TBZ and FBZ at low level concentrations in interfering media. Water is used as carrier, and a 40% v/v methanol–water mixture (eluent solution) is the only organic solvent involved in the experimental procedure.

Among the second-order algorithms analyzed, U-PLS/RBL allowed the successful determination of both analytes even in the presence of three real interferences. This is a new example of the power of coupling the partial-least-squares algorithm and residual bilinearization.

Since the excitation-emission matrices are measured by a fast-scanning spectrofluorimeter, the global time involved in the determination is not seriously affected. Taking into account this fact, we can state that in the proposed methodology the advantages of the flow-analysis are added to the sensitivity of fluorescence solid-matrix methods and to the selectivity of the second-order multivariate calibration.

Acknowledgements

Universidad Nacional de Rosario, CONICET (Consejo Nacional de Investigaciones Científicas y Técnicas, Project PIP 1950), and ANPCyT (Agencia Nacional de Promoción Científica y Tecnológica, Project PAE-22204) are gratefully acknowledged for financial support.

References

1 G. M. Escandar, *Fungicides: Chemistry, Environmental Impact and Health Effects*, P. De Costa and P. Bezerra (Eds) Nova Science Publishers, New York, 2009, Ch. 7.
2 European Comission, document SANCO/2007/3131, *Method Validation and Quality Control Procedures for Pesticide Residues Analysis in Food and Feed*, 31 October 2007.
3 Website of the United State Environmental Protection Agency (U.S. EPA): www.epa.gov/pesticides/.
4 V. Andreu and Y. Picó, *TrAC, Trends Anal. Chem.*, 2004, **23**, 772–789.
5 C. Soler and Y. Picó, *TrAC, Trends Anal. Chem.*, 2007, **26**, 103–115.
6 C. C. Leandro, P. Hancock, R. J. Fussell and B. J. Keely, *J. Chromatogr., A*, 2007, **1144**, 161–169.
7 K. A. Fletcher, S. O. Fakayode, M. Lowry, S. A. Tucker, S. L. Neal, I. W. Kimaru, M. E. McCarroll, G. Patonay, P. B. Oldham, O. Rusin, R. M. Strongin and I. M. Warner, *Anal. Chem.*, 2006, **78**, 4047–4068.
8 G. N. Piccirilli and G. M. Escandar, *Analyst*, 2006, **131**, 1012–1020.
9 C. Bosch Ojeda and F. Sánchez Rojas, *Sensors*, 2006, **6**(10), 1245–1307.
10 J. F. García Reyes, E. J. Llorent Martínez, P. Ortega Barrales and A. Molina Díaz, *Anal. Chim. Acta*, 2006, **557**, 95–100.
11 X. Wang, M. L. Liu, X. L. Cheng and J. M. Lin, *TrAC, Trends Anal. Chem.*, 2009, **28**, 75–87.
12 S. Matsuokaa and K. Yoshimura, *Anal. Chim. Acta*, 2010, **664**, 1–18.
13 J. F. García Reyes, P. Ortega Barrales and A. Molina Díaz, *Anal. Chim. Acta*, 2003, **493**, 35–45.
14 J. F. García Reyes, P. Ortega Barrales and A. Molina Díaz, *J. Agric. Food Chem.*, 2004, **52**, 2197–2202.
15 J. F. García Reyes, E. J. Llorent Martínez, P. Ortega Barrales and A. Molina Díaz, *Anal. Bioanal. Chem.*, 2004, **378**, 429–437.
16 J. F. García Reyes, E. J. Llorent Martínez, P. Ortega Barrales and A. Molina Díaz, *Talanta*, 2004, **64**, 742–749.
17 E. J. Llorent Martínez, J. F. García Reyes, P. Ortega Barrales and A. Molina Díaz, *J. AOAC Int.*, 2005, **88**, 860–865.
18 A. Domínguez Vidal, P. Ortega Barrales and A. Molina Diaz, *J. Fluoresc.*, 2007, **17**, 271–277.
19 K. S. Booksh and B. R. Kowalski, *Anal. Chem.*, 1994, **66**, 782A–791A.
20 Å. Rinnan, J. Riu and R. Bro, *J. Chemom.*, 2007, **21**, 76–86.
21 G. M. Escandar, N. M. Faber, H. C. Goicoechea, A. Muñoz de la Peña, A. C. Olivieri and R. J. Poppi, *TrAC, Trends Anal. Chem.*, 2007, **26**, 752–765.
22 A. C. Olivieri, *Anal. Chem.*, 2008, **80**, 5713–5720.
23 A. Valero Navarroa, P. C. Damiani, J. F. Fernández Sánchez, A. Segura Carretero and A. Fernández Gutiérrez, *Talanta*, 2009, **78**, 57–65.
24 R. Bro, *Chemom. Intell. Lab. Syst.*, 1997, **38**, 149–171.
25 J Öhman, P. Geladi and S. Wold, *J. Chemom.*, 1990, **4**, 135–146.
26 A. C. Olivieri, *J. Chemom.*, 2005, **19**, 253–265.
27 R. Bro, *J. Chemom.*, 1996, **10**, 47–61.
28 *MATLAB 7.0*, The Mathworks, Natick, MA, 2000.
29 http://www.models.kvl.dk/source/.
30 A. C. Olivieri, H. L. Wu and R. Q. Yu, *Chemom. Intell. Lab. Syst.*, 2009, **96**, 246–251.
31 www.chemometry.com.
32 J. López Flores, M. L. Fernández de Córdova and A. Molina Diaz, *Anal. Sci.*, 2009, **25**, 681–686.
33 P. C. Tway and L. J. Cline Love, *J. Phys. Chem.*, 1982, **86**, 5227–5230.
34 A. Lopes, A. L. Maçanita, F. S. Pina, E. Melo and H. Wamhoff, *Environ. Sci. Technol.*, 1992, **26**, 2448–2453.
35 D. Picón Zamora, M. Martínez Galera, A. Garrido Frenich and J. L. Martínez Vidal, *Analyst*, 2000, **125**, 1167–1174.
36 M. J. Rodríguez Cuesta, R. Boqué, F. X. Rius, D. Picón Zamora, M. Martínez Galera and A. Garrido Frenich, *Anal. Chim. Acta*, 2003, **491**, 47–56.
37 S. A. Bortolato, J. A. Arancibia and G. M. Escandar, *Anal. Chem.*, 2008, **80**, 8276–8286.
38 J. A. Arancibia, C. E. Boschetti, A. C. Olivieri and G. M. Escandar, *Anal. Chem.*, 2008, **80**, 2789–2798.
39 D. Bohoyo Gil, A. Muñoz de la Peña, J. A. Arancibia, G. M. Escandar and A. C. Olivieri, *Anal. Chem.*, 2006, **78**, 8051–8058.
40 P. C. Damiani, I. Durán Merás, A. G. García Reiriz, A. Jiménez Jirón, A. Muñoz de la Peña and A. C. Olivieri, *Anal. Chem.*, 2007, **79**, 6949–6958.
41 R. Bro and H. L. Kiers, *J. Chemom.*, 2003, **17**, 274–286.
42 A. G. González, M. A. Herrador and A. G. Asuero, *Talanta*, 1999, **48**, 729–736.
43 D. M. Haaland and E. V. Thomas, *Anal. Chem.*, 1988, **60**, 1193–1202.
44 R. Jorgensen Casella, S. Garrigues, R. E. Santelli and M. de la Guardia, *Analyst*, 2000, **125**, 257–261.
45 J. Sancenón and M. de la Guardia, *Anal. Chim. Acta*, 1994, **287**, 49–57.
46 A. Heredia and M. J. Bukovac, *J. Agric. Food Chem.*, 1992, **40**, 2290–2293.
47 M. J. Ruedas Rama, A. Ruiz Medina and A. Molina Diaz, *Anal. Chim. Acta*, 2002, **459**, 235–243.
48 G. N. Piccirilli and G. M. Escandar, *Anal. Chim. Acta*, 2009, **646**, 90–96.
49 F. García Sánchez and A. Aguilar Gallardo, *Microchem. J.*, 1994, **50**, 161–168.

